ISSN 1330–0008
CODEN FIZAE4

SPECTROSCOPIC PROPERTIES OF THE Li, Zn METALS AND Li-Zn ALLOY PLASMAS GENERATED BY XeCl-LASER ABLATION

SREĆKO GOGIĆ AND SLOBODAN MILOŠEVIĆ

Institute of Physics, P.O. Box 304, HR-10000 Zagreb, Croatia
E-mail: slobodan@ifs.hr, Fax: 00 385 1 4680 399

Received 23 December 1997; revised manuscript received 30 April 1998
Accepted 25 May 1998

Using 308 nm laser ablation, we have produced lithium, zinc and lithium-zinc plasmas and have studied their spectral, temporal and spatial characteristics. In pure lithium plume, linear Stark effect is observed in n^2D-2^2P transitions ($n = 3, 4, 5, 6$) up to 0.3 μs after the laser pulse. In pure zinc plume, both atomic and ionic spectral lines are observed. Time evolution of spectral line intensities suggests that the mechanism responsible for population of atomic zinc states is a cascade of ion-electron recombination processes. The ablation of Li-Zn alloy shows much faster decay of Zn spectral features than of Li spectral lines. Therefore, the decomposition of plume into shells of different colours is observable.

PACS number: 52.50.Jm UDC 537.53

Keywords: laser ablation, Li, Zn and Li-Zn plasmas, spectral, temporal and spatial characteristics of plumes

1. Introduction

The Li-Zn system, the simplest example among alkali-metal-group-IIB molecules, has been studied recently by preparing excited molecules within heat-pipe ovens through the photochemical reactions [1]. These studies have indicated the need of preparing excimers in molecular beams [2, 3] in order to achieve state-specific excitation. However, when

lithium and zinc are mixed in the oven, high temperature of the alloy is needed to obtain a sufficient vapour pressure for an appropriate expansion and cooling of molecules in the beam [4]. The expansion of laser-generated plasma through an orifice is a widely used method to produce cold molecules from the alloys which have a high melting temperature and a low vapour pressure of one of the elements [5, 6]. Such a source can also produce excited dimer molecules directly in the laser-generated plume, as observed in the case of Pb_2 [7], Na_2 [8] and Cu_2 [9].

The pulsed lithium atomic beam was produced by CO_2-laser-induced ablation of a Li metal target in the low-energy-density regime when no plasma forms on the surface, in order to study collisions of lithium Rydberg atoms with buffer gases [10, 11]. The ablation of lithium and zinc has also been used in various applications such as a matrix isolation spectroscopy (lithium) [12] or in basic studies of ablation process of metals (zinc) [13, 14]. The laser ablation of multicomponent targets [15] suggests that different ablation processes could be expected when dealing with alloys such as LiZn.

We have undertaken the present study with the aim to characterize plumes formed by 308 nm XeCl-laser ablation of lithium, zinc and lithium-zinc targets. We observed the spectra of laser-generated plume and performed their temporal and spatial analyses for various buffer gases and laser fluences. Preliminary results have been reported recently [16].

2. Experiment

The experimental setup is shown in Fig. 1. A XeCl-excimer laser at 308 nm was used for ablation. The laser energy could be varied up to 150 mJ per pulse and the pulse halfwidth was about 20 ns. The laser beam, which is initialy 2 cm x 1 cm, was focused by a quartz lens of a 30 cm focal length, producing a waist of about 80 μm on the target surface, with a maximum power of about 10^5 MW/cm^2. Calibrated quartz plates were used to reduce the fluence. The target was placed inside a small vacuum chamber (10 ℓ) which could be evacuated by a Roots pump system down to 10^{-4} mbar and/or filled with different gases (Ar, He, H_2) up to atmospheric pressure. The light from the plume was projected onto the plane of the opening of a bundle optical fiber (diameter 3 mm) by a lens. The optical fiber was connected to a 0.6 m scanning monochromator. Spectrally dispersed fluorescence was detected by a photomultiplier (Hamamatsu R2949). The signal was sent to a box-car averager (Stanford Research Model 250) where it was processed and the output was sent to an IBM compatible PC. A fast photodiode, collecting the scattered laser light, was used to trigger the gate of a box-car averager at a certain time delay after the beginning of the laser pulse. Signals from the photomultiplier and from the gate of the box-car averager were monitored with a 100 MHz oscilloscope. The temporal selection of the measured spectra could be achieved in the range from about 20 ns to 15 μs after the laser pulse. Spatial, temporal and spectral analyses of the plume were performed. The spatial analysis was performed by selecting a certain position of the opening of the optical fiber along the image of the plume. The temporal particular set of delay and gate parameters while scanning the monochromator, or by setting the monochromator at the wavelength of the desired spectral

feature while scanning the delay of the box-car gate.

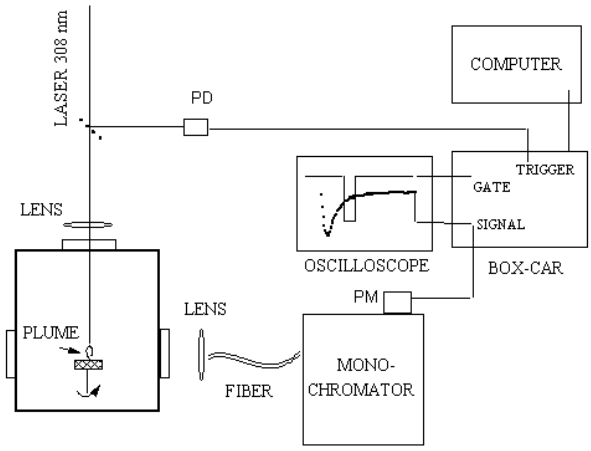

Fig. 1. Experimental setup for laser ablation of lithium, zinc and LiZn *alloy targets.*

The spectral response of the system was measured with a calibrated tungsten ribbon lamp. The spectral response curve is almost flat from 400 nm to 600 nm, decreasing linearly to 20% at 800 nm. The spectra shown in Figs. 2, 5 and 7 were not corrected for the spectral response of the system.

The targets were pure lithium, zinc metal and their alloys. The alloys were prepared in heat-pipe ovens [1]. The targets were rotated in order to get uniform plumes. That was especially important for lithium since the laser beam easily creates a crater in the target which causes spatial instability of the plume.

3. Results and discussion

When the laser pulse hits the surface of the target, it vaporizes and ionizes the material. Looking with the naked eye (time-averaged picture), the light-emitting plasma changes shape when the buffer gas and/or its pressure are changed. Under vacuum conditions ($P < 10^{-2}$ mbar), a bright white spot is observed at the place were the laser hits the target. Very low intensity emission (blue or green) extends in almost the whole vacuum chamber. When a buffer gas is introduced into the chamber, the region of this weak emission suddenly starts to shrink and forms a small bright ball of emitting light (of 5 to 15 mm diam. at 2 - 5 mbar). This ball of light can have shells of different colours (e.g. ablation of LiZn alloy creates green inner and reddish outer shells). As the buffer gas pressure is increased (at about 100 mbar), the ball shrinks into a small very bright white spot on the target surface. Small evaporated particles of a size of a few micrometers that were leaving the target, could be seen with the naked eye in the incoming laser beam.

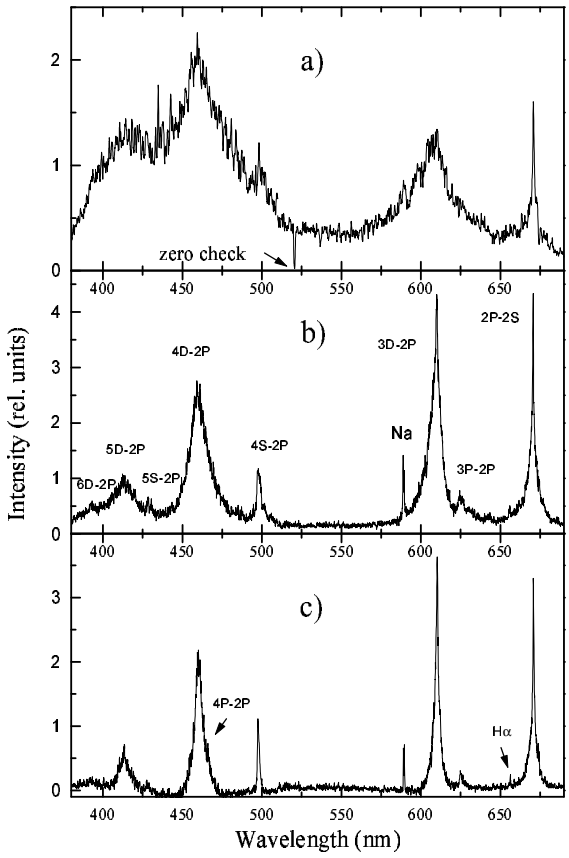

Fig. 2. Spectra of lithium plasma for different time delays in Ar *buffer gas at the pressure of 5* mbar*. The light from the complete plume of about 1* cm *in diameter was fed to the monochromator. G is the gate and D the delay setting of the box-car averager. a)* $D = 30$ ns*,* $G = 100$ ns*; b)* $D = 130$ ns*,* $G = 100$ ns *c)* $D = 230$ ns*,* $G = 100$ ns*. Laser-pulse energy was 25* mJ*.*

3.1. Ablation of pure lithium metal

The plume of lithium plasma is observed for a laser-pulse energy above 10 mJ. In Fig. 2 we present spectra of the excimer-laser generated lithium plasma in the region from 390 nm to 690 nm for different time delays after the beginning of the laser pulse, integrated over 100 ns. The light from the entire bright ball was fed into the fiber. In that spectral range, only neutral lithium atomic spectral features could be seen. For short time intervals after the laser pulse (up to 100 ns), continuum emission is observed due to the spectral overlap of highly broadened atomic lines. The most prominent effect can be seen as a broadening of the n ^{2}D $\rightarrow$ 2 ^{2}P transitions ($n = 3, 4, 5, 6$), while the n ^{2}S $\rightarrow$ 2 ^{2}P transitions ($n = 4,\ 5$) exibit weaker broadening with a slight red asymmetry. The forbidden 3,4 ^{2}P $\rightarrow$ 2 ^{2}P

transitions were also observed. The n ^{2}D $\rightarrow$ 2 ^{2}P transitions are symmetric and their full-width at half maximum (FWHM) reaches 12 nm at a time delay of 30 ns. The linewidths were found to increase almost linearly when increasing laser pulse energy or the buffer gas pressure, and decrease exponentially with increasing time delay. The observations indicate a high electron density within the first few hundred nanoseconds after the laser pulse. Similar plasma conditions were obtained by Ya'akobi [17] by the method of an exploding lithium wire. The main broadening mechanism has been explained as the linear Stark effect. Preliminary comparison shows that the electron densities of 10^{17}–10^{18} cm^{-3} are obtained in the present

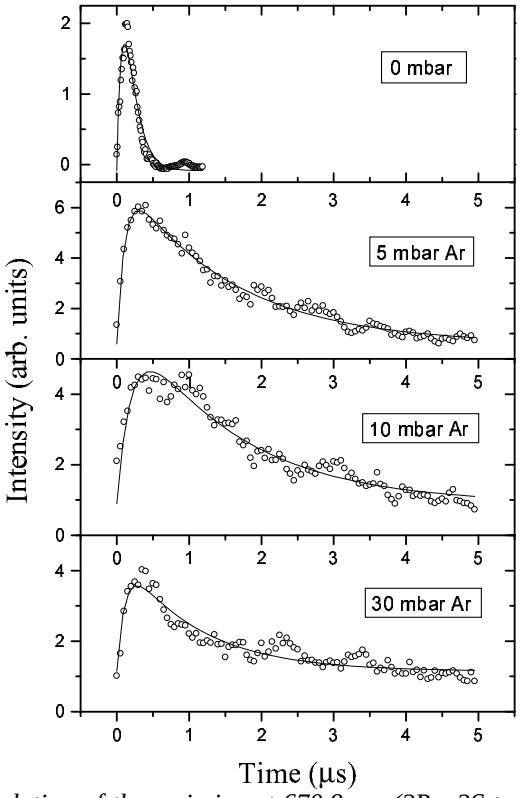

Fig. 3. Temporal evolution of the emission at 670.8 nm *(2P→2S transition) for different argon buffer-gas pressures. Gate width was 6* ns *and laser-pulse energy was 25* mJ.

case. We note that in experiments with an exploding lithium wire, the self-reversal on the line shapes [18] is readily observed. The light trapping is definitely present also in the present experiment, however, the self-reversal in the 2P $\rightarrow$ 2S line shape is observed only above 500 mbar buffer-gas pressure.

Figure 3 shows typical time evolutions of the 670.8 nm fluorescence (2P $\rightarrow$ 2S transition) for different argon buffer gas pressures. They were obtained with the monochromator set in the spectral wing of the 2P $\rightarrow$ 2S resonance transition and by scanning the delay of

the box-car gate which was 6 ns wide. We note that the intensities shown in Figs. 2 and 3 can not be easily compared due to different integration times.

In order to analyze the observed dependence of $I(t)$, we assume a simple model which describes the pumping and decaying mechanism of the 2P upper state. The rate of change of the upper state is given by

$$\frac{\mathrm{d}N_{2P}}{dt} = N(t)\Gamma - N_{2P}(t)\Gamma_{2P}, \tag{1}$$

where $N(t)$ is the total density of excited atoms decaying to the 2P state with the effective decay constant Γ. Assuming $N(t) = N_0\ \mathrm{e}^{-t/\tau_1}$, $N_{2P}(0) = 0$ and with

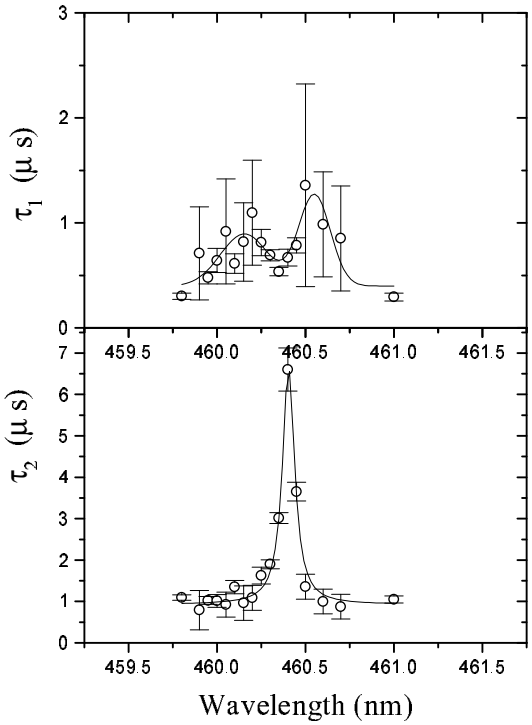

Fig. 4. The time constants τ_1 and τ_2 for the 460.3 nm *line in* Ar *buffer-gas at pressure of 10* mbar*. Laser-pulse energy was 25* mJ*.*

$\Gamma = \frac{1}{\tau_1}, \Gamma_{2P} = \frac{1}{\tau_2}$, the solution is

$$N_{2P}(t) \propto \frac{\tau_2}{\tau_2 - \tau_1}(e^{-\frac{t}{\tau_2}} - e^{-\frac{t}{\tau_1}}) \tag{2}$$

The full line in Fig. 3 shows the result of the fit of the functional form given by Eq. (2). In this particular case, the satisfactory fit proves the assumption of the above model, namely,

that one dominant pumping process exists. The effective lifetime, τ_2, at zero buffer gas pressure is found to be about 100 ns. It increases to about 1.5 μs when the buffer gas (argon) is introduced into the chamber at pressure between 5 and 10 mbar. At higher pressure of about 30 mbar, it decreases to about 1 μs. It is interesting to note that this dependence appears to be closely correlated with the sudden formation of the light ball and its shrinking as the buffer-gas pressure is increased. Since the natural lifetime of the 2P $\rightarrow$ 2S transition is only 27 ns [19], the large decay times are obviously due to the long pumping time of the 2P level and due to the radiation trapping effect at higher buffer gas pressures. It is striking that the simple model presented above gives a good description of the observed intensities, since the 2P level population is obviously under influence of cascades from higher lithium atomic levels. If dominant, cascade contributions or several pumping mechanisms with different rates would give rise to slower decay of fluorescence in its tail (see for example Eq. (3) in Ref. 20). We assume that Li(2P) atoms are dominantly produced directly through electron-ion recombination into the 2P state. However, lithium ionic lines could not be observed in the present experiments to support the existence of excited lithium ions, because most prominent lines are in the deep UV region, and a few lines available in the visible part of the spectrum are masked by the Stark broadened 4D $\rightarrow$ 2P transition at 460 nm.

On the oscilloscope, we observe a large change of time evolution of the fluorescence while scanning the monochromator around 460 nm. In order to clarify this observation, the effective lifetimes were measured within the line profile of the 4D $\rightarrow$ 2P transition at 460.3 nm. For each setting of the monochromator in the linewing of the 4D $\rightarrow$ 2P transition, the time dependence of emission was measured, and the curves such as those shown in Fig. 3 were obtained. In Fig. 4, we show the result of the fit, namely, the values of the parameters τ_1 and τ_2, versus wavelength in the region of the line profile. We note that the natural lifetime of the 4D level is (31 ± 1) ns [21]. The parameter τ_1 should reflect a typical time of the processes which populate 4D level. It is between 0.5 to 1 μs. It is possible that a certain structure in the dependence of $\tau_1(\lambda)$ exists, but large error bars do not allow a conclusion. The display of the parameter τ_2 versus wavelength (lower part of Fig. 4) shows almost Lorentzian shape with a halfwidth of about 0.09 nm. (The spectral resolution of the monochromator is about 0.02 nm). Typical lifetimes in the wings of the line profiles are about 1 μs. For example, at 5 nm from the line center, the linear Stark broadening is dominant (see Fig. 2), hence we can conclude that the measured effective lifetime τ_2 at that wavelength reflects a lifetime of a high-electron-density plasma. In the center of the line, the effective lifetime amounts 5–7 μs which is most likely due to the light trapping (high density of atoms in 2P states) but also to the prolonged filling of the 4D level.

3.2. Ablation of pure zinc metal

With a target of pure zinc, similar spatial shapes of plumes were observed, however, of different colours (predominantly blue). Figure 5 shows typical spectra in the spectral range from 400 to 700 nm. The spectrum shown in Fig. 5a was taken at a small time delay after the laser pulse, with the narrow gate of the box-car averager, selecting through the fiber only the light from the almost white nucleus of the plume. Both atomic and ionic lines

of zinc were observed within 300 ns after the laser pulse. The ionic transition $4\,^2F_{7/2} \rightarrow 4\,^2D_{5/2}$ at 492.3 nm shows a pronounced Stark broadening suitable for diagnostics. Figure 5b shows the spectrum when only light from the outer ball was fed through the fiber. Only lines of atomic zinc stemming from metastable $4p\,^3P_{0,1,2}$ levels were observed. Comparing the observations of temporal evolutions with pure zinc and pure lithium, it appears that recombination processes responsible for the spectral emission from the plasma are faster in zinc than in the pure lithium.

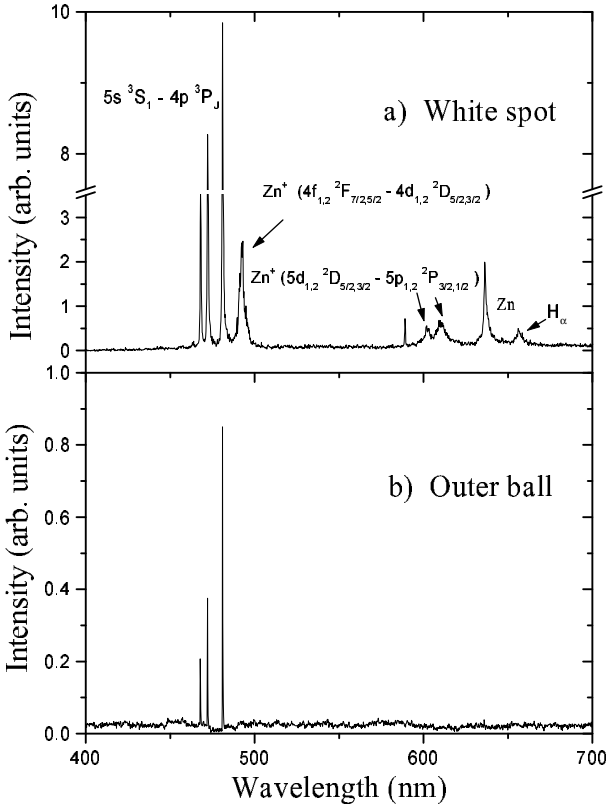

Fig. 5. Spectra of excimer-laser generated zinc plasma in the H_2 *buffer gas at 6* mbar. *a) taken from the white spot, D = 100* ns, *G = 100* ns*; b) from the outer ball, D = 100* ns, *G = 3* μs. *Laser-pulse energy was* 115 mJ.

Figure 6 shows temporal evolution of atomic zinc emission at 481.05 nm from different spatial regions in (a) H_2 and (b) He atmosphere. The temporal evolution of the white spot intensity is characterized by a strong peak at the time delay of about 250 ns and a long tail which can also be seen as a well developed second maximum at 3 μs (Fig. 6b). Temporal evolution of the outer ball exhibits only one maximum shifted to about 800 ns or 4000 ns, depending on the buffer gas. Neither the white spot nor the outer ball temporal evolutions can be described by the simple model given above. Rather, the second maximum appears to be the result of a chain of reactions preceding the population of the relevant upper

state. Most probably, Zn^+ ions recombine with electrons giving rise to the population of long-lived Rydberg states of Zn which radiatively fill the upper state of the observed transition. This long-lived intermediate state seems to cause the secondary maximum of the fluorescence signal.

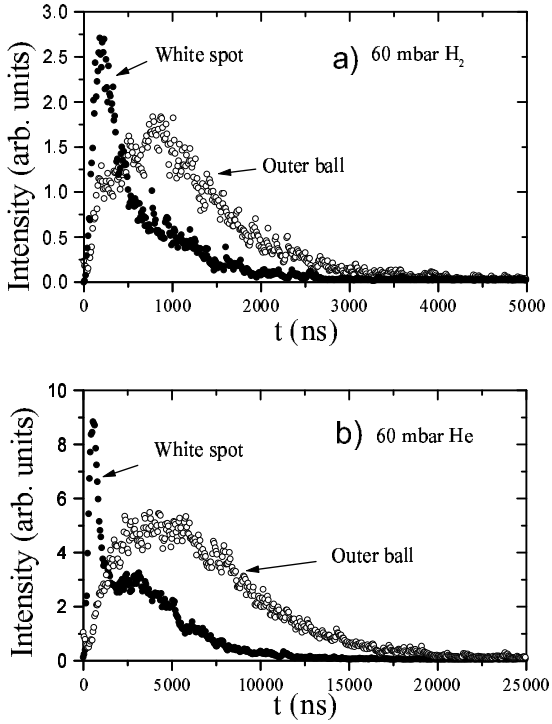

Fig. 6. Temporal evolution of characteristic emission at 481.05 nm *from specific spatial regions of excimer-laser generated zinc plasma a) with* H_2 *buffer gas at 60* mbar *and b) with* He *buffer gas at 60* mbar. *Laser pulse energy was 115* mJ.

We note that with the helium buffer gas, larger light intensities were obtained with a considerably larger characteristic lifetime of the emission compared to the case of H_2 buffer gas. This was observed both for the white spot and the outer ball. We believe that the molecular buffer gas is more efficient in quenching the plasma compared to the atomic buffer gas [10]. We note that we have observed a weak emission from atomic hydrogen which could be an indication that reaction processes are also taking place. However, no excited molecular products could be observed (for example ZnH). That does not exclude creation of products in the ground state.

3.3. Ablation of lithium-zinc metal alloy

We performed ablation of the lithium-zinc metal alloy that was prepared in the heat-pipe oven [1]. Its composition (about 50:50 molar ratio) was found suitable for photo-

chemical production of LiZn excimers. Figure 7 shows spectra of lithium-zinc metal alloy plume in the spectral range of 450 nm to 500 nm, for different time delays after the laser pulse. This particular spectral range was chosen because the blue-green colours dominate the main portion of the plume, and also because LiZn excimer emission is expected at 470 nm [1]. The presence of excited LiZn molecules was not detected. The reason for that could be that multicomponent plasma is

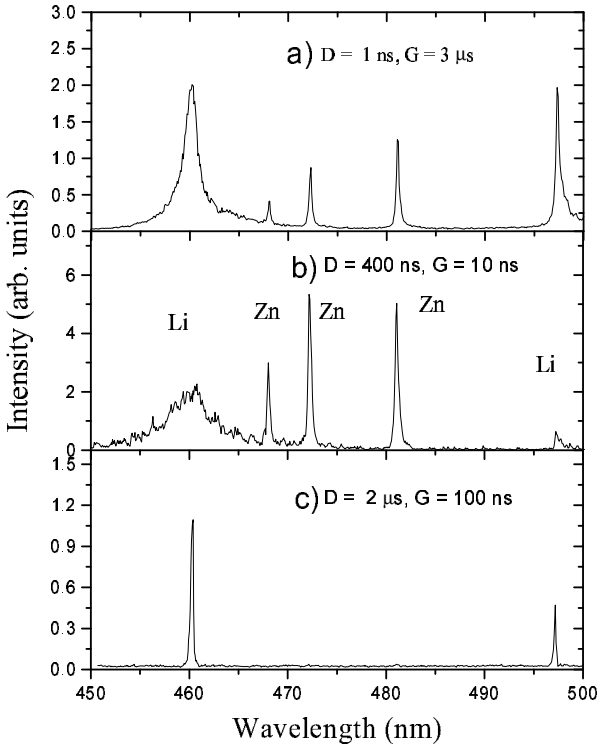

Fig. 7. Spectra from the excimer-laser generated plasma of Li-Zn *alloy in argon at 67* mbar *for different settings of the delay and gate of the box-car averager. Laser-pulse energy was 115* mJ.

flying apart due to a large mass difference of Li and Zn, and when it becomes cold enough to allow formation of molecules, the density of both components at the same time and place is too low. This could be overcome by preparing an alloy of specific composition. We note that in the case of pure lithium and pure zinc, we were not able to detect spectra of the excited dimer Li_2 or Zn_2 molecules, in a wide range of time delays and space.

From Fig. 7, one can see that lithium spectral features persist for a much longer time. This is the main reason for the spatial regions of the plume with different colours in the case of laser ablation of the Li-Zn alloys, namely reddish outer shell ($2P \rightarrow 2S$ transition, not shown in Fig. 7).

4. Conclusions

The ablation of lithium metal with the 308 nm beam laser results in the formation of plasma for laser pulse energies above about 10 mJ. The plasma is of low atomic density but with high electron densities, which causes pronounced broadening of the nD $\rightarrow$ 2P lithium transitions by the linear Stark effect. An unusual time evolution of the fluorescence within the 4D $\rightarrow$ 2P line profile was observed which is considered to be an interplay of effects of radiation trapping due to large Li(2P) population and the linear Stark broadening due to a high electron density. The ablation of zinc targets leads to the formation of multiply ionized atoms, which then recombine forming the highly excited atoms and less ionized atoms. This is reflected in the formation of different colour balls and of layers around the point where the laser beam hits the surface.

Acknowledgements

This work was financially supported by the Ministry of Science and Technology of the Republic of Croatia. We wish to thank Dr. Goran Pichler for valuable discussions and continuous support in this work.

References

1) S. Milošević, X. Li, D. Azinović, G. Pichler, M. C. van Hemert, A. Stehouwer and R. Düren, J. Chem. Phys. **96** (1992) 7364;
2) S. Milošević, in *Spectral Line Shapes*, Vol. 8, eds. A. D. May, J. R. Drummond and E. Oks, (AIP Conf. Proc. 328, AIP Press, New York, 1995) pp. 391–405 and references therein;
3) D. Azinović, X. Li, S. Milošević and G. Pichler, Phys. Rev. A **53** (1996) 1323;
4) T. B. Massalski, ed., *Binary Alloy Phase Diagrams* (Am. Soc. for Metals, Metals Park, Ohio, 1986), Vol. 2, p. 1511;
5) J. B. Paul, J. J. Scherer, C. P. Collier and R. J. Saykally, J. Chem. Phys. **104** (1996) 2782;
6) J. S. Pilgrim and M. A. Duncan, Chem. Phys. Lett. **232** (1995) 335;
7) V. E. Bondybey and J. H. English, J. Chem. Phys. **74** (1981) 6978;
8) C. W. Huie and E. S. Yeung, Spectrochimica Acta **40B** (1985) 1225;
9) R. W. Dreyfus, J. App. Phys. **69** (1991) 1721;
10) B. Dubreuil and M. Harnafi, Phys. Rev. **40** (1989) 69;
11) M. Harnafi and B. Dubreuil, J. Appl. Phys. **69** (1991) 7565;
12) M. E. Fajardo, J. Chem. Phys. **98** (1993) 110;
13) V. K. Goncharov, V. I. Karaban, V. L. Kontsevoĭ and T. V. Stasyulevich, Sov. J. Quantum Electron. **21** (1991) 790;
14) J. M. Green, W. T. Silfvast and O. R. Wood II, J. App. Physics **48** (1977) 2753;
15) R. Koppmann, S. M. Refaei and A. Paspieszczyk, J. Vac. Sci. Technol. A **4** (1986) 79;
16) S. Gogić and S. Milošević, in *Spectral Line Shapes*, Vol. 9, eds. M. Zoppi and L. Ulivi (AIP Conf. Proc. 386, AIP Press, New York, 1997) p. 163-166;
17) B. Ya'akobi Phys. Rev. **176** (1968) 227;

18) B. Ya'akobi J. Quant. Spectrosc. Radiat. Transfer. **9** (1969) 1097;

19) A. Gaupp, P. Kuske and H. J. Andrä, Phys. Rev. A **26** (1982) 3551;

20) C. J. Bowers, D. Budker, E. D. Commins, D. DeMille, S. J. Freedman, A.-T. Nguyen, S.-Q. Shang and M. Zolotorev, Phys. Rev. A **53** (1996) 3103;

21) J. Heldt and G. Leuchs, Z. Phys. A **291** (1979) 11.

SPEKTORSKOPSKA SVOJSTVA PLAZME METALA LITIJA I CINKA I Li–Zn LEGURA PROIZVEDENIH ABLACIJOM POMOĆU XeCl LASERA

Proučavali smo spektralna, vremenska i prostorna svojstva litijeve, cinkove i litij-cink plazme stvorene ablacijom pomoću lasera na 308 nm. Kod čistog litija opažen je pri n^2D-2^2P prijelazima ($n = 3, 4, 5, 6$) linearni Starkov efekt u vremenu do 0.3 μs nakon laserskog pulsa. Kod čistog cinka opažene su i atomske i ionske spektralne linije. Na temelju vremenske evolucije intenziteta spektralnih linija može se zaključiti da je mehanizam naseljavanja pobuđenih stanja atoma cinka kaskada rekombinacijskih procesa između iona i elektrona. Pri ablaciji litij-cink slitine opaženo je mnogo brže gušenje zinkovih spektralnih pojava nego litijevih. To je glavni razlog razdvajanja oblačka litij-cink plazme u ljuske različitih boja.